

Article

A Series of New Manganese(II) Polynuclear Complexes Based on Nitrothiacalix[4]arenes: The Study of Interplay between Macrocyclic Platform Flexibility and Structural Diversity of Coordination Compounds

Alexander S. Ovsyannikov ^{1,*}, Iuliia V. Strelnikova ¹, Ilya D. Shutilov ¹, Daut R. Islamov ², Pavel V. Dorovatovskii ³, Aidar T. Gubaidullin ⁴, Artem S. Agarkov ⁴, Svetlana E. Solovieva ¹ and Igor S. Antipin ^{1,*}

- ¹ Kazan Federal University, Kremlevskaya 18 Str., Kazan 420008, Russia; jstrelnikova@yandex.ru (I.V.S.); iliyashutilov308@gmail.com (I.D.S.); evgersol@yandex.ru (S.E.S.)
- ² Laboratory for Structural Analysis of Biomacromolecules, Kazan Scientific Center of Russian Academy of Sciences, Lobachevskogo 2 Str., Kazan 420008, Russia; daut1989@mail.ru
- ³ National Research Centre "Kurchatov Institute", Acad. Kurchatov 1 Sq., Moscow 123182, Russia; paulgemini@mail.ru
- ⁴ Arbuzov Institute of Organic and Physical Chemistry, FRC Kazan Scientific Center, Russian Academy of Sciences, Arbuzova 8, Kazan 420088, Russia; aidar@iopc.ru (A.T.G.); artem.agarkov.95.chem@mail.ru (A.S.A.)
- * Correspondence: osaalex2007@rambler.ru (A.S.O.); iantipin54@yandex.ru (I.S.A.)



Citation: Ovsyannikov, A.S.; Strelnikova, I.V.; Shutilov, I.D.; Islamov, D.R.; Dorovatovskii, P.V.; Gubaidullin, A.T.; Agarkov, A.S.; Solovieva, S.E.; Antipin, I.S. A Series of New Manganese(II) Polynuclear Complexes Based on Nitrothiacalix[4]arenes: The Study of Interplay between Macrocyclic Platform Flexibility and Structural Diversity of Coordination Compounds. *Crystals* **2023**, *13*, 1017. <https://doi.org/10.3390/cryst13071017>

Academic Editor: Ana M. Garcia-Deibe

Received: 31 May 2023

Revised: 19 June 2023

Accepted: 21 June 2023

Published: 26 June 2023



Copyright: © 2023 by the authors. Licensee MDPI, Basel, Switzerland. This article is an open access article distributed under the terms and conditions of the Creative Commons Attribution (CC BY) license (<https://creativecommons.org/licenses/by/4.0/>).

Abstract: Four new manganese(II) complexes, based on dinitro and tetranitrothiacalix[4]arenes, were synthesized and characterized from structural points of view in the crystalline phase. It was revealed that thiacalix[4]arenes decorated with two and four electron withdrawing groups, when combined with MnCl₂, afforded the formation of similar tetranuclear complexes **1** and **2a** with two non-equivalent metal ions and a rhombic geometry of the metallic cluster core. The distortion of the coordination sphere of metal cations within the obtained complexes was found to be dependent on the number of nitro groups located at the upper rim of the macrocyclic backbone, adopted in cone conformation. The tetranuclear complex **2b** of a different type, displaying the formation of a dinuclear cluster core, crystallized in a non-centrosymmetric space group was obtained, when tetranitrothiacalix[4]arene, adopted in a partial cone conformation, was involved in coordination with manganese(II) cations. The switching of coordination behavior for the macrocyclic ligand in **2b** was achieved due to the presence of upper-rim-disposed electron-withdrawing nitro groups, increasing the flexibility of the macrocyclic backbone by breaking the H-bonding between the OH phenolate moieties within the ligand structure. Finally, the use of 2,2'-bipyridine as an auxiliary ligand in coordination with tetranitrothiacalix[4]arene and manganese(II) cations led to the third type complex formation **3**, where the macrocycle platform adopted in a 1.2-alternate conformation.

Keywords: thiacalix[4]arenes; manganese(II) complexes; clusters; nitro derivatives; partial cone; supramolecular chemistry; X-ray diffraction; self-assembly

1. Introduction

Calix[4]arenes [1–3] are a class of macrocyclic compounds composed of four phenolate moieties connected together by methylene bridges (CA), thioether (TCA) [4] or sulfonyl groups (SO₂CA) [5] (see Figure 1). Due to annular rotation around C–C or C–S single bonds imposed by the steric repulsion of aryl moieties, these macrocycles can adopt four limited conformations: cone (A), partial cone (paco) (B), 1.2-alternate (C), and 1.3-alternate (D) (see Figure 2). In solution as well as in the crystalline phase, the conformations for non-substituted calix[4]arene derivatives can be stabilized by H-bonding, occurring between the OH-phenolate groups: for cone conformation the formation of cyclic four-center H-bonds

is observed, whereas one three-center and two two-center H-bonds are involved in a partial cone conformation and 1.2-alternate conformation stabilization, respectively. Finally, the 1.3-alternate conformation is realized when the steric repulsion of aryl units is a dominating factor influencing the conformation behavior of the macrocycle backbone. Earlier, crystal structure studies revealed that for **CA** [6] and **TCA** [7], the cone conformation is more stable in the crystalline phase. On the contrary, the appearance of strong electron-withdrawing groups such as SO_2 bridges in the **SO₂CA** structure leads to the weakening of the H-bonding between the OH phenolate groups, leading to the formation of the 1.3-alternate conformation in the crystalline phase [8].

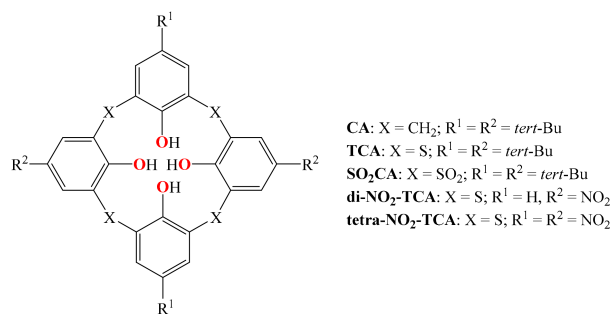


Figure 1. The calix[4]arene family of polydentate ligands.

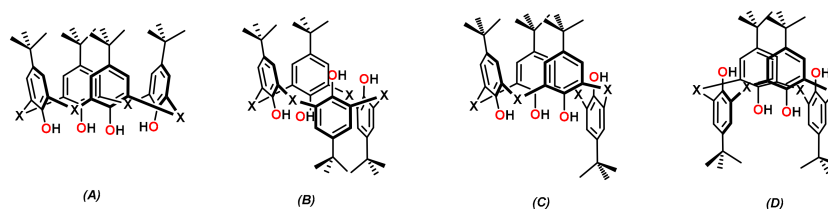


Figure 2. Four possible limited conformations of the macrocyclic platform for calix[4]arene family of ligands (X = CH₂, S, SO₂): cone (A), partial cone (paco) (B), 1.2-alternate (C), and 1.3-alternate (D).

It is important to note that the stabilization of the macrocyclic backbone conformation can also be achieved by using not only H-bonding but coordination bonding with metal ions. Over the last few decades, the coordination chemistry of calix[4]arene-based compounds presenting the formation of cluster complexes of different nuclearities, involving 3d as well as 4f metal ions, has been intensively studied [9,10]. A growing interest to such types of coordination compounds has evolved due to the smart properties that these complexes exhibit. In particular, it was shown that the conventional “classical” calix[4]arene demonstrates a strong ability to coordinate with manganese (II/III) cations, leading to the formation of discrete cluster complexes displaying intriguing magnetic properties, such as single molecular behavior [11–13] or the magnetic calorimetry effect [14]. It should be mentioned that for all reported 3d and 4f metal complexes, the macrocycle adopts only a cone conformation serving as a “cap” for the stabilization of obtained polynuclear species [15–18]. For this reason, the **CA** ligand and its functional derivatives can be considered as rather conformationally rigid ligands.

As expected, whereas **CA** and **TCA** are prone to adopt only cone conformation upon the formation of polymetallic coordination species with 3d and 4f metal ions [19–25], **SO₂CA** demonstrates more flexible conformational behavior when binding with metal ions, adopting cone [26] as well as 1.2-alternate conformations [27,28]. It is important to note that the 1.3-alternate conformation (D) was observed mostly for the *d*-metal coordination polymers [29–31] based on the lower-rim modified **CA/TCA** ligands. To the best of our knowledge, no evidence of coordination compounds, displaying the macrocyclic ligands, adopted in a partial cone conformation (C), was reported to date.

It was shown that **TCA**- and **SO₂CA**-based 3d and 4f metal complexes can exhibit not only attractive magnetic [28], but luminescence properties [32–34]. For a series of

SO₂CA-based manganese (II,III) complexes [35], green–red luminescence was revealed, related with prohibited *d-d** electron transitions, thus evidencing the significant role of the electron structure of the macrocyclic ligand with respect to the observed physical properties of the complexes. Some of obtained polynuclear coordination species based on **TCA** were useful for (photo)catalytic application [36]. In addition, the interaction of **TCA** and **SO₂CA** ligands (L) with M(II) ions (especially, Co²⁺, Ni²⁺ and Zn²⁺) can also lead to generated [M₄L]⁴⁺ “shuttlecock”-like secondary building blocks in situ due to their involving an interaction with metal ions S- or O-atoms from the bridging groups with the following formation of porous coordination cages [37–44] or polymers [45–48] upon self-assembly with polytopic carboxylic or pyrazolyl compounds, finding applications as porous materials, which proves the wide range interest in the design of calix[4]arene-based supramolecular solid-state architectures.

As already mentioned, physical properties, such as magnetic behavior or luminescence, of the coordination complexes are strongly dependent on the coordination environment of the metallic centre and the ligand field that can be tuned up by the insertion of functional groups, displaying different electron-withdrawing or donating effects. In particular, the presence of electron-withdrawing groups may straighten or weaken the coordination bonding with the metallic ion, thus leading to a drastic change in its magnetic behavior. Concerning the calix[4]arene family of the ligands (see Figure 1), the study of the influence of the withdrawing groups grafted at the para position, with respect to the OH-phenolate coordinating centres, on their coordination ability towards 3d or 4f metal ions has not been reported.

In this contribution, we report on the formation and X-ray diffraction study of a series of new manganese(II) complexes based on thiacalix[4]arenes, bearing two and four nitro groups, disposed at the upper rim of the macrocycle backbone (**di-NO₂-TCA** and **tetra-NO₂-TCA**, respectively), which allows for a better understanding of the influence of upper-rim-disposed electron-withdrawing groups on the conformation flexibility of macrocycle ligands and performs the fine tuning of the coordination environment of 3d metal ions. The elucidation of the structural change of the coordination sphere of manganese(II) ions within the obtained complex is of a high importance from the application point of view and may pave the way for the further investigation in this field.

2. Materials and Methods

2.1. Materials and Characterization Methods

All chemicals were purchased from commercial suppliers and used without additional purification. Solvents were purified according to standard protocols. Dinitro and tetranitrothiacalix[4]arene (**di-NO₂-TCA** and **tetra-NO₂-TCA**) were synthesized by following the reported procedure [49,50].

Infrared spectra (IR) of powdered crystalline samples in KBr were recorded on a Tensor 27 Fourier-transform spectrometer (Bruker, Germany) in a range of 4000–400 cm^{−1} with an optical resolution of 4 cm^{−1} and an accumulation of 32 scans.

Elemental analysis was performed on a EuroEA 3028-HT-OM Eurovector S.p.A. (Pavia, Italy).

2.2. Crystallization Conditions

2.2.1. Synthesis of [Mn^{II}₄(di-NO₂-TCA)₂(DMF)₄] 2DMF (1)

Dinitrothiacalix[4]arene (**di-NO₂-TCA**) (0.02 g, 0.03 mmol) and MnCl₂ · 4H₂O (0.027 g, 0.13 mmol) were mixed in DMF/MeOH solution (*v/v* = 1/1, 20 mL), followed by triethylamine addition (0.039 mL, 0.27 mmol), affording a yellow solution. The reaction mixture was stirred at room temperature for 1 h and then filtered out. The vapor diffusion of *i*-PrOH into filtrate induced the formation of crystals, suitable for X-ray diffraction analysis, for 1 month. The yield of the complex was 30%, based on p-dinitrothiacalix[4]arene. IR (ν , cm^{−1}): 2926(m), 2855(m), 1655(s), 1648(s), 1639(s), 1571(m), 1459 (m), 1451(s), 1326(m), 1281(m), 1131(m), 1064(m), 844(w), 796(w), 767(w), 744(w), 713(w). Elemental analysis for

$C_{66}H_{62}Mn_4N_{10}O_{22}S_8$, Anal. Calcd.: C, 43.47%; H, 3.43%; N, 7.68%; Found: C, 43.90%; H, 3.89%; N, 8.53%.

2.2.2. Synthesis of $[Mn^{II}_4(\text{tetra-NO}_2\text{-TCA})_2(\text{DMF})_4] \cdot 4Et_2O$ (**2a**)

Tetranitrothiacalix[4]arene (**tetra-NO₂-TCA**) (0.03 g, 0.044 mmol) $MnCl_2 \cdot 4H_2O$ (0.035 g, 0.177 mmol) were mixed in DMF/MeOH solution ($v/v = 1/1$, 10 mL), followed by triethylamine addition (0.16 mL, 1.15 mmol). The solution color turned light brown. The reaction mixture was stirred at room temperature for 1 h and then filtered out. The crystals of complex **2a**, suitable for X-ray diffraction analysis, were formed after the vapor diffusion of Et_2O into filtrate for 1 month. The yield of complex **2a** was 52% based on tetranitrothiacalixarene. IR (ν , cm^{-1}): 3070 (w), 2982 (w), 2931(w), 1654(s), 1566(s), 1462(s), 1338(w), 1332(s), 1140(s), 1067(w), 914(m), 835(w), 765(m), 746(m), 714 (m). Elemental analysis for $C_{68}H_{64}Mn_4N_{12}O_{30}S_8$, Anal. Calcd.: C, 40.72%; H, 3.22%; N, 8.38%; Found: C, 41.58%; H, 3.59%; N, 8.08%.

2.2.3. Synthesis of $[Mn^{II}_4(\text{tetra-NO}_2\text{-TCA})_2(\text{DMF})_8]$ (**2b**)

Tetranitrothiacalix[4]arene (**tetra-NO₂-TCA**) (0.03 g, 0.044 mmol) and $MnCl_2 \cdot 4H_2O$ (0.035 g, 0.177 mmol) were mixed in DMF/MeOH solution ($v/v = 1/1$, 10 mL), followed by the triethylamine addition (0.16 mL, 1.15 mmol). The solution color turned light brown. The reaction mixture was stirred at room temperature for 1 h. The crystals of **2b**, suitable for X-ray diffraction analysis, were formed after the vapor diffusion of *i*-PrOH into filtrate for 1 month. The yield of complex **2b** was 22% based on tetranitrothiacalixarene. IR (ν , cm^{-1}): 3071(w), 2928(w), 1654 (m), 1566(m), 1460(m), 1386(w), 1336(s), 1184(w), 1139(m), 1066(w), 914(w), 833(w), 766(w), 746(w), 713(w). Elemental analysis for $C_{78}H_{90}Mn_4N_{18}O_{34}S_8$, Anal. Calcd.: C, 40.73%; H, 3.94%; N, 10.96%; Found: C, 41.25%; H, 4.08%; N, 11.12%.

2.2.4. Synthesis of $[Mn^{II}_2(\text{tetra-NO}_2\text{-TCA})(\text{bipy})_2(\text{DMF})_2]$ (**3**)

Tetranitrothiacalix[4]arene (**tetra-NO₂-TCA**) (0.052 g, 0.07 mmol), 2,2'-bipyridine (**bipy**) (0.087 g, 0.56 mmol) and $MnCl_2 \cdot 4H_2O$ (0.0915 g, 0.4 mmol) were mixed in DMF/MeOH solution ($v/v = 1/1$, 10 mL) and then triethylamine was added (0.183 mL, 1.23 mmol). The solution color turned orange. The reaction mixture was stirred at room temperature for 1 h. The formed precipitate was filtered out and dissolved in DMF. The crystals of **3**, suitable for X-ray diffraction analysis, were obtained upon the slow evaporation of the DMF solution. The yield of **3** was 55% based on tetranitrothiacalixarene. IR (ν , cm^{-1}): 3070 (w), 2929(w), 1660(s), 1595(m), 1557(s), 1487(s), 1439(s), 1407(w), 1385(m), 1334(s), 1301(s), 1177(w), 1136(s), 1058(m), 1016(m), 916(m), 831(m), 762(m), 748(w), 738(w), 715(m). Elemental analysis for $C_{50}H_{38}Mn_2N_{10}O_{14}S_4$, Anal. Calcd.: C, 48.39%; H, 3.09%; N, 11.29%; Found: C, 48.49%; H, 3.32%; N, 11.36%.

2.3. Crystallographic Data Collection and Refinement

Diffraction data for single crystals of **1** and **2a** were collected at 100 K on the 'Be-lok/XSA' beamline ($\lambda = 0.745 \text{ \AA}$, 0.7454 \AA for **1** and **2a**, respectively, φ -scans) of the Kurchatov Synchrotron Radiation Source (Moscow, Russia) [51,52]. Diffraction patterns were collected using a Mardtb goniometer equipped with Rayonix SX165 2D positional sensitive CCD detector at 100 K. In total, 300 frames were collected with an oscillation range of 1° . The data were indexed, integrated and scaled; absorption correction was applied using the XDS program package [53]. The structures were solved by direct methods with the software SHELXT [54]. The structural model was investigated and refined using Olex2 software [55] with a full-matrix least-squares method on F² with anisotropic displacement. All hydrogen atoms were placed in calculated positions and included in the refinement within the riding model with fixed isotropic displacement parameters $U_{iso}(H) = 1.5U_{eq}(O)$, $1.2U_{eq}(N)$, and $1.2U_{eq}(C)$. For **1**, since there was a high disordering of solvent molecules located in the pores, the Solvent Mask command generated by the BYPASS module within Olex 2 software [55] was applied to calculate 740 electrons per unit cell within solvent-accessible

voids of 1398.7 \AA^3 (16.4%) determined by PLATON analysis [56]. The recovered number of electrons can correspond to an unidentifiable number and composition of solvate molecules comprising DMF, MeOH, iso-propanol, and H_2O .

Diffraction data for single crystals of **2b** were collected on a Rigaku XtaLab Synergy S instrument with a HyPix detector and a PhotonJet microfocuss X-ray tube using $\text{Cu-K}\alpha$ (1.54184 \AA) radiation at 100 K. The reflections were indexed and integrated according to the diffraction patterns using the CrysAlisPro data reduction package. Data were corrected for systematic errors and absorption using the ABSPACK module. The GRAL module was used for the analysis of systematic absences and space group determination. Using Olex 2 software [55], the structure was solved by direct methods with SHELXT [54] and refined by the full-matrix least-squares method on F^2 using SHELXL [57]. A solvent mask was calculated and 140 electrons were found in a void volume of 692 \AA^3 per unit cell. This is consistent with the presence of one isopropanol molecule per asymmetric unit which counts 136 electrons per unit cell. Non-hydrogen atoms were refined anisotropically. The hydrogen atoms were inserted at the calculated positions and refined as riding atoms.

Diffraction data for single crystals of **3** were collected on a Bruker D8 Quest single crystal X-ray diffractometer equipped with an Incoatec $\text{I}\mu\text{S}$ microfocuss source ($\text{Mo K}\alpha$, $\lambda = 0.71073 \text{ \AA}$), a multilayers optics monochromator, and a PHOTON III area detector, in the ω - and φ -scan modes at 100 K. The frames were integrated with the Bruker SAINT software package using a narrow-frame algorithm. Data were corrected for absorption effects using the Multi-Scan method by the SADABS program [58]. The structure was solved by a direct method using SHELXS and refined by the full-matrix least-squares method using SHELXTL programs [59]. All non-hydrogen atoms were refined anisotropically. The positions of the hydrogen atoms were determined based on the electronic density distribution and were refined as riding atoms. For data collection, the frames were indexed and integrated using the APEX3 data reduction package [60]. All calculations were performed on PC using the WinGX suit of programs [61,62].

The crystallographic data for **1**, **2a**, **2b** and **3** are gathered in Table 1.

Table 1. Crystallographic data and structure refinement details for the compounds **1**, **2a**, **2b** and **3**.

Compound Name	1	2a	2b	3
Empirical formula	$\text{C}_{60}\text{H}_{48}\text{Mn}_4\text{N}_8\text{O}_{20}\text{S}_8$, 2($\text{C}_3\text{H}_7\text{NO}$)	$\text{C}_{60}\text{H}_{44}\text{Mn}_4\text{N}_{12}\text{O}_{28}\text{S}_8$, 4($\text{C}_4\text{H}_{10}\text{O}$)	$\text{C}_{72}\text{H}_{72}\text{Mn}_4\text{N}_{16}\text{O}_{32}\text{S}_8$, 3($\text{C}_3\text{H}_7\text{NO}$)	$\text{C}_{50}\text{H}_{38}\text{Mn}_2\text{N}_{10}\text{O}_{14}\text{S}_4$
Formula weight (g/mol)	1823.49	2153.79	2222.79	1241.02
Wavelength, \AA	0.745 (synchrotron)	0.7454 (synchrotron)	1.54178	0.71073
Temperature	100(2)	100(2)	100(1)	100(2)
Crystal system	monoclinic	monoclinic	orthorhombic	monoclinic
Space group	$\text{C}2/c$	$\text{P}2_1/n$	$\text{Pca}2_1$	$\text{P}2_1/n$
$a/\text{\AA}$	34.619(7)	18.524(4)	30.9394(3)	11.6426(14)
$b/\text{\AA}$	15.323(3)	12.704(3)	16.75530(10)	10.3239(12)
$c/\text{\AA}$	18.704(4)	19.494(4)	18.9143(2)	21.412(2)
$\alpha/^\circ$	90	90	90	90
$\beta/^\circ$	120.86(3)	103.59(3)	90	94.661(3)
$\gamma/^\circ$	90	90	90	90
$V, \text{\AA}^3$	8517(4)	4459.0(16)	9805.15(15)	2565.2(5)
Z, Z'	4, 0.5	2, 0.5	4	2, 0.5
$\rho_{\text{calc}} \text{ g/cm}^3$	1.422	1.604	1.506	1.607
μ, cm^{-1}	0.958	0.941	6.443	7.34
$F(000)$	3728.0	2216.0	4560.0	1268
Crystal size, mm	$0.32 \times 0.21 \times 0.14$	$0.33 \times 0.25 \times 0.15$	$0.19 \times 0.15 \times 0.12$	$0.34 \times 0.15 \times 0.13$
2θ range for data collection/ $^\circ$	$3.134 \leq 2\theta \leq 61.986$ $-47 \leq h \leq 47$ $-20 \leq k \leq 20$ $-25 \leq l \leq 25$	$4.048 \leq 2\theta \leq 62.046$ $-25 \leq h \leq 25$ $-17 \leq k \leq 15$ $-26 \leq l \leq 26$	$5.274 \leq 2\theta \leq 152.986$ $-34 \leq h \leq 39$ $-21 \leq k \leq 18$ $-22 \leq l \leq 22$	$3.818 \leq 2\theta \leq 61.094$ $-16 \leq h \leq 16$ $-14 \leq k \leq 14$ $-30 \leq l \leq 30$
Index ranges				
Reflections collected/independ.	48,978/11,583	43,236/12,068	55,374/16,302	44,904/7836
R_{int}	0.0596	0.0418	0.0388	0.0447
Completeness to $\theta_{\text{max}}/\%$	98.3	97.8	97.1	99.7
Data/restraints/parameters	11,583/2/516	12,068/0/603	16,302/1/1253	7836/0/363
Goodness-of-fit on F^2	1.046	1.020	1.078	1.055
Final R indexes [$I > 2\sigma(I)$]	0.0542/0.1469	0.0390/0.0967	0.0428/0.1171	0.0363/0.0908
$R1/wR2$				
Final R indexes (all data)	0.0798/0.1607	0.0546/0.1051	0.0441/0.1181	0.0453/0.1000
$\rho_{\text{max}}/\rho_{\text{min}} (\text{e}\text{\AA}^{-3})$	0.57/−0.62	0.48/−0.79	0.56/−0.48	0.553/−0.640
Flack parameter	-	-	0.361(3)	-

The crystallographic data are available for free-of-charge downloading from the Cambridge Crystallographic Data Centre via www.ccdc.cam.ac.uk/datarequest/cif (accessed on 20 June 2023). CCDC Numbers: 2,265,060 (**1**), 2,265,061 (**2a**), 2,265,062 (**2b**) and 2,260,192 (**3**), respectively.

3. Results

3.1. Syntheses and General Aspects

The synthesis of crystals of **1** and **2b** suitable for single crystal X-ray diffraction was achieved by the slow vapor diffusion of the iso-propanol into the DMF/MeOH solution ($v/v = 1/1$) containing the dissolved compounds **di-NO₂-TCA** or **tetra-NO₂-TCA** (1 equiv.), MnCl₂ salt (4 equiv.) and triethylamine (10 equiv.). For **2a**, the monocrystals were synthesized as described for **1** and **2b**, but the diethyl ether was used instead of iso-propanol upon the vapor's diffusion. Finally, the crystals of **3** were obtained when the 2,2'-bipyridine (equiv.) was added to the reaction mixture composed of dissolved compound **2**, MnCl₂ and triethylamine in the same molar ratio, as mentioned above, followed by recrystallisation from the DMF solution (see Section 2).

3.2. Crystal Structure Analysis

Complex **1** crystallizes in the monoclinic $C2/c$ space group giving rise to crystal formula [C₆₀H₄₈Mn₄N₈O₂₀S₈] 2(C₃H₇NO) and is composed of two tetra-deprotonated **di-NO₂-TCA** molecules, four manganese atoms, six DMF solvate molecules (see Figure 3a, Table 1). There are two non-equivalent manganese atoms in the asymmetric unit. The first one, Mn(1), adopting the distorted trigonal prismatic (TPR-6) coordination sphere [63] (see Table S2), is bound with four O-atoms and two S-atoms, belonging to two adjacent macrocycle molecules (see Figure 3b, Tables S1 and S2 see in Supplementary Materials). In contrast, the Mn(2) atom is octacoordinated and adopts a biaugmented trigonal prismatic coordination sphere (JBTPR-8) [63] (see Table S3), in which four O-atoms come from phenolate groups and two S-atoms come from two macrocyclic molecules and two O-atoms from coordinated DMF molecules (see Figure 3b, Table S1). According to bond lengths analysis (see Table S1) and the charge balance, all manganese atoms, presenting in the tetranuclear cluster node, are in the +II oxidation state as in the used metal salt (MnCl₂). The Mn(1) and Mn(2) atoms form the flat rhomb with sides equal to 3.499(1) Å and 3.523(1) Å, respectively, and angles 104.59(2)° (for Mn(1)) and 75.41(2)° (for Mn(2)). The **di-NO₂-TCA** behaves as a tetra-tridentate ligand, bonding with four Mn(II) cations, by offering three coordination pockets composed of two μ_2 -O-phenolate atoms and one S-atom. The macrocycle backbone adopts a pinched cone conformation, which is identified by the dihedral angles between the opposite aryl units equal to 69.17° and 49.50°. Moreover, the coordination of **di-NO₂-TCA** with manganese(II) cations leads to the screwing of the macrocycle's opposite aryl units respecting the axis, passing through the C(8), C(4) C(12), and C(16) atoms, resulting in the formation of torsion angles equal to -9.1(2)° and 8.5(2)°, respectively (see Figure S2a).

For **1**, the hydrophobic cavity of **di-NO₂-TCA** accommodates the DMF molecule due to weak CH/ π interactions between the methyl group and its thiacalix[4]arene aryl units ($d_{\text{CH}_3 \dots \text{C}_{6\text{centroid}}} = 3.631$ Å and 3.547 Å, respectively) (Figure S3a). The DMF molecules are found to be disordered over two positions with occupancies 0.54/0.46.

In the crystal of **1**, the complex species forms 2D layers supported by O(DMF) ... S, C-H ... S, C-H(DMF) ... C(DMF), C-H ... O(nitro) intermolecular interactions along the $y0z$ plane (see Figure 4). Within the layer, the coordination species of **1** display a perpendicular orientation: the dihedral angle formed by the planes, passing through four Mn(II) atoms, belonging to each {Mn₄}-cluster unit is found to be equal to 89° (see Figure S4). The 2D layers are stacked along the $0x$ axis completing the 3D crystal packing with the pores occupied by the disordered solvent molecules, which were not refined (see Section 2).

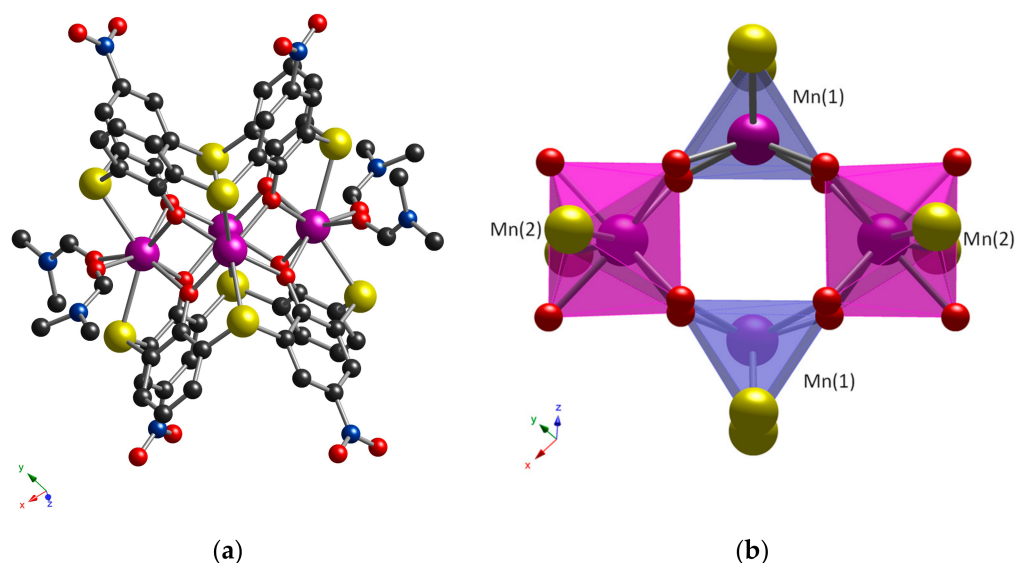


Figure 3. Crystal structure of **1** (a) and its rhombic tetranuclear {Mn₄}-cluster unit (b) demonstrating the coordination environment of Mn(1) and Mn(2) atoms. The C-, N-, O-, Mn- and S-atoms are represented by black, blue, red, purple and yellow spheres, respectively. Hydrogen atoms and DMF solvate molecules are omitted for clarity.

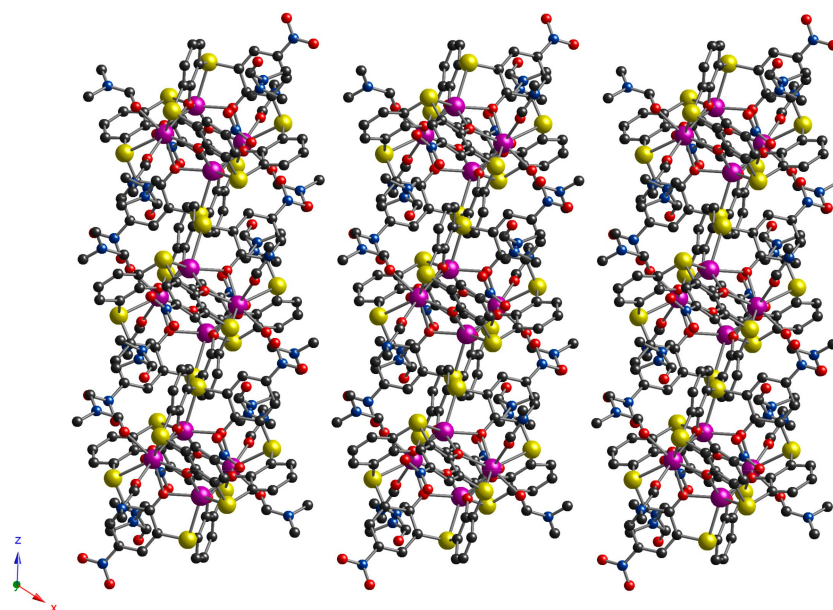


Figure 4. A portion of crystal packing of **1** showing the parallel stacking of the supramolecular noncovalent-bonded 2D layers along y_0z plane. The C-, N-, O-, Mn- and S-atoms are represented by black, blue, red, purple and yellow spheres, respectively. Hydrogen atoms are omitted for clarity.

Complex **2a**, very similar to **1** from a structural point of view, crystallizes in the monoclinic $P2_1/n$ space group, leading to crystal formula $[C_{60}H_{44}Mn_4N_{12}O_{28}S_8] 4(C_4H_{10}O)$ (see Table 1, Figure 5a). The structure of **2a** is also composed of a tetranuclear {Mn₄}-cluster core hold between two molecules of **tetra-NO₂-TCA** ligand. As for **1**, four DMF molecules are found to be coordinated to manganese(II) atoms at both side positions. There are four non-equivalent manganese(II) atoms, displaying the coordination environment/sphere similar to those of **1**: O₄S₂ (Mn(1)) and O₆S₂ (Mn(2)) (see Figure 5b). On the other hand, the corresponding Mn(1)-S bonds are found to be slightly stronger, while Mn(1)-O coordination

bonds are relatively weaker when compared to those observed for **1** (see Table S1). For the Mn(2) atoms, the coordination bonds formed between μ_2 -O-phenolate atoms of the macrocycle backbone and Mn(II) atoms are also relatively weaker than in **1**, but, surprisingly, it was revealed that the coordination bonding with O-atoms belonging to DMF molecules is enhanced with a remarkable difference of ca. 0.02–0.05 Å. As a result, it is worth noting that such a change in coordination behavior influences the corresponding coordination bonds' characteristics (length and angles) involving the Mn(2) atoms and O(DMF)-atoms. Moreover, due to the enhancement in the coordination bonding of the Mn(2) atoms with DMF molecules, a significant elongation of corresponding Mn(2)-S bonds is observed for **2a**, compared to those found for **1**. Four manganese atoms are located in the same plane forming the rhomb with a distorted geometry, compared to this one described for **1**. The distances between the Mn(1) and Mn(2) atoms are 3.532(1) Å and 3.5744(8) Å, respectively. The Mn(2)-Mn(1)-Mn(2) and Mn(1)-Mn(2)-Mn(1) angles are found to be equal to 105.40(1)° and 74.60(1)°, respectively. This means that the {Mn₄}-cluster node for **2a** is relatively compressed along the Mn(1)-Mn(1) axis and stretched respecting to the Mn(2)-Mn(2) axis (see Figure 5b) compared to the one of **1**.

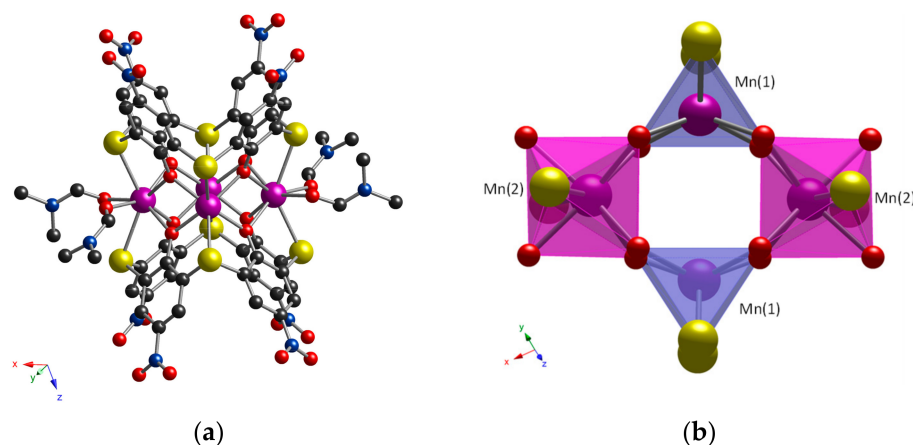


Figure 5. Crystal structure of **2a** (a) and rhombic tetranuclear {Mn₄}-cluster unit (b) demonstrating the coordination environment of Mn(1) and Mn(2) atoms. The C-, N-, O-, Mn- and S-atoms are represented by black, blue, red, purple and yellow spheres, respectively. Hydrogen atoms and DMF solvate molecules are omitted for clarity.

The **tetra-NO₂-TCA** demonstrates the same coordination mode when binding with the Mn(II) ions in **2a** as the **di-NO₂-TCA** ligand in **1**, providing four tri-dentate OSO-pockets. All phenolic O-atoms are deprotonated, giving rise to an overall charge for the ligand [**tetra-NO₂-TCA**]⁴⁻. Despite **tetra-NO₂-TCA** displaying very similar values of dihedral angles between the opposite aryl units of the macrocycle backbone (66.05° and 46.18°), compared to **di-NO₂-TCA**, the enhanced distortion of the **tetra-NO₂-TCA** platform, caused by the screwing of the macrocycle backbone along the axis connecting C(1) and C(4) atoms as well as C(12) and C(6) atoms, leading to torsion angles of −11.7(1)° and 10.7(1)°, respectively, is observed (see Figure S2b). Due to weak CH/ π interactions, the hydrophobic cavity of both coordinated **tetra-NO₂-TCA** molecules forms the inclusion complex with one molecule of diethyl ether with a 1/1 ratio ($d_{C15 \dots C6_{\text{centroid}}} = 3.621$ Å and $d_{C31 \dots C6_{\text{centroid}}} = 3.648$ Å, respectively, see Figure S3b).

In terms of crystal packing, the molecules of **2a** are arranged in an *anti*-parallel fashion along the *Oy* axis, forming the channels fielded by solvate molecules of diethyl ether, which demonstrate the weak CH/ π bonding of nitroaryl thiacalix[4]arene moieties from the outward side (see Figures 6 and S5) ($d_{C(35) \dots C6_{\text{centroid}}} = 3.670$ Å).

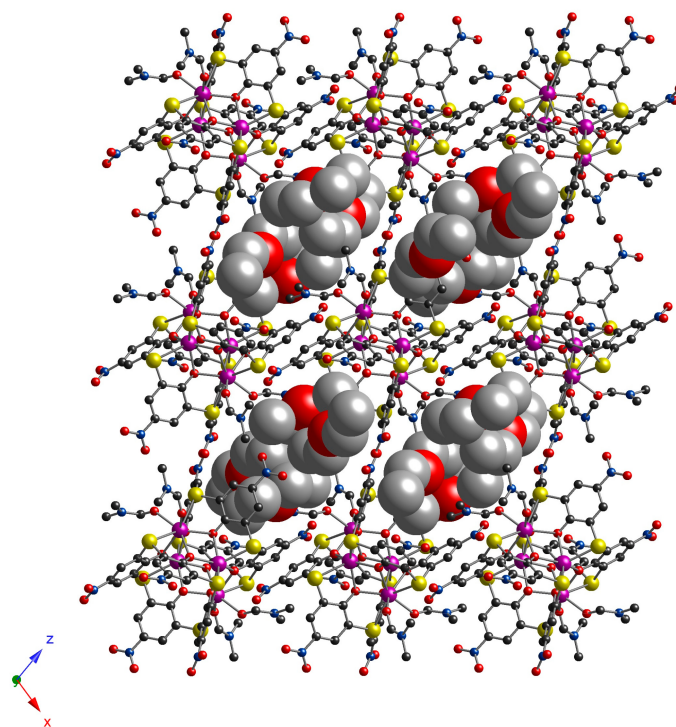


Figure 6. A portion of crystal packing of **2a** showing the formation of 1D channels along $0y$ axis filled by diethyl ether molecules. The C-, N-, O-, Mn- and S-atoms are represented by black, blue, red, purple and yellow spheres, respectively. Hydrogen atoms are omitted for clarity. The diethyl ether molecules are represented by large grey and red spheres.

Complex **2b** crystallizes in the non-centrosymmetric $Pca2_1$ space group of the orthorhombic system and is of the formula $[C_{72}H_{72}Mn_4N_{16}O_{32}S_8, C_3H_7NO]$ (see Figure 7, Tables 1 and S1). The complex structure demonstrates a completely different coordination pattern and is formed by two thiacalix[4]arene ligands, four Mn ions, and solvate DMF molecules. The distinctive feature of **2b** is the macrocyclic ligand, adopted in a less symmetric *paco* conformation, when coordinating to metal ions, which is, to the best of our knowledge, the first evidence of thiacalix[4]arene-based metal complexes in the crystalline phase. On one side, the **tetra-NO₂-TCA** behaves as monodentate ligand, when binding with Mn(3) and Mn(4) atom and *bis*-tridentate ligand, offering two adjacent OSO cavities for coordination with two Mn(1) and Mn(2) atoms. As a result, the Mn(3) and Mn(4) atoms are located in the centers of the trigonal bipyramids (see Table S4) and display a very similar O₅-coordination environment composed of one O-atom of the phenolate group of the thiacalix[4]arene backbone and four O-atoms belonging to four coordinated DMF solvate molecules. The Mn(1) and Mn(2) atoms, disposed in the central part of the complex, coordinate with both molecules of the macrocyclic ligand, adopting a distorted trigonal prismatic coordination sphere [63] (see Table S2), filled by four O-atoms of the phenolate groups (of which two are μ_2 -O-bonding atoms) and two S-atoms (see Figure 7b, Table S1). One of the four DMF molecules coordinated to the Mn(1) and Mn(2) atoms is oriented inward, respecting the macrocyclic hydrophobic cavity, displaying intermolecular CH/ π -bonding with one of three nitroaryl moieties ($d_{C_{56} \dots C_{6\text{centroid}}} = 3.574 \text{ \AA}$).

In the crystal of **2b**, the self-assembly of complex species leads to the formation of a 3D molecular network, resulting from various weak CH/ π -, CH/O(nitro) interactions (see Figures 8 and S6).

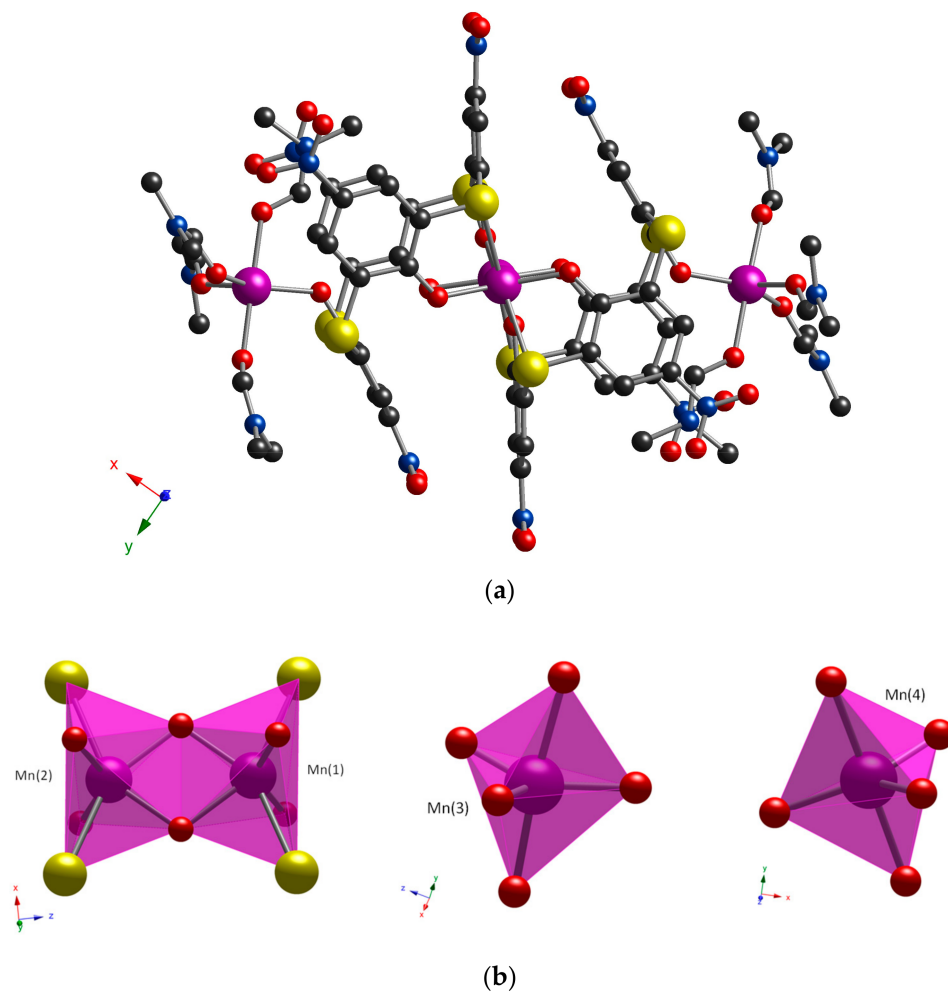


Figure 7. For **2b**, a crystal structure (a) and coordination environment of Mn atoms (b). The C-, N-, O-, Mn- and S-atoms are represented by black, blue, red, purple and yellow spheres, respectively. Hydrogen atoms are omitted for clarity.

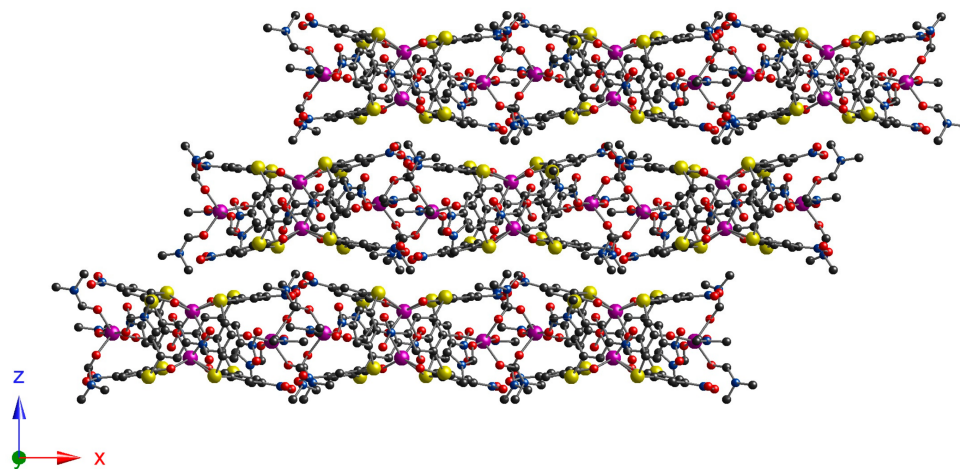


Figure 8. A portion of 3D crystal packing of **2b** (view along $0y$ axis). The C-, N-, O-, Mn- and S-atoms are represented by black, blue, red, purple and yellow spheres, respectively. Hydrogen atoms are omitted for clarity.

The combination of **tetra-NO₂-TCA**, MnCl₂ and 2,2'-bipyridine (**bipy**) bearing N,N-donor chelate coordinating group led to the formation of complex **3** presenting the crystal formula [C₅₀H₃₈Mn₂N₁₀O₁₄S₄] (see Figure 9a, Tables 1 and S1). The crystal structure of **3** is composed of one molecule of **tetra-NO₂-TCA**, two Mn(II) atoms, two **bipy** molecules, and two DMF molecules. There is only one non-equivalent Mn(1) atom, presenting in the +II oxidation state and coordinated with two O-atoms and one S-atom, belonging to two phenolate groups and thioether junctions of the macrocycle backbone, one O-atom of DMF molecule, and two N-atoms coming from the **bipy** molecule, leading to the N₂O₂S distorted octahedral coordination sphere (see Figure 9b, Tables S1 and S2). The macrocyclic ligand adopted in the *1.2-alternate* conformation displayed a parallel orientation of the opposite aryl rings of the molecular platform, offering two OSO pockets for the formation of coordination bonds when binding with the Mn(II) ions. The Mn(1) atoms are symmetrically disposed, with respect to the two O-phenolate atoms, with 2.083(1) Å and 2.085(1) Å bond distances, respectively (see Figure 9b, Table S1).

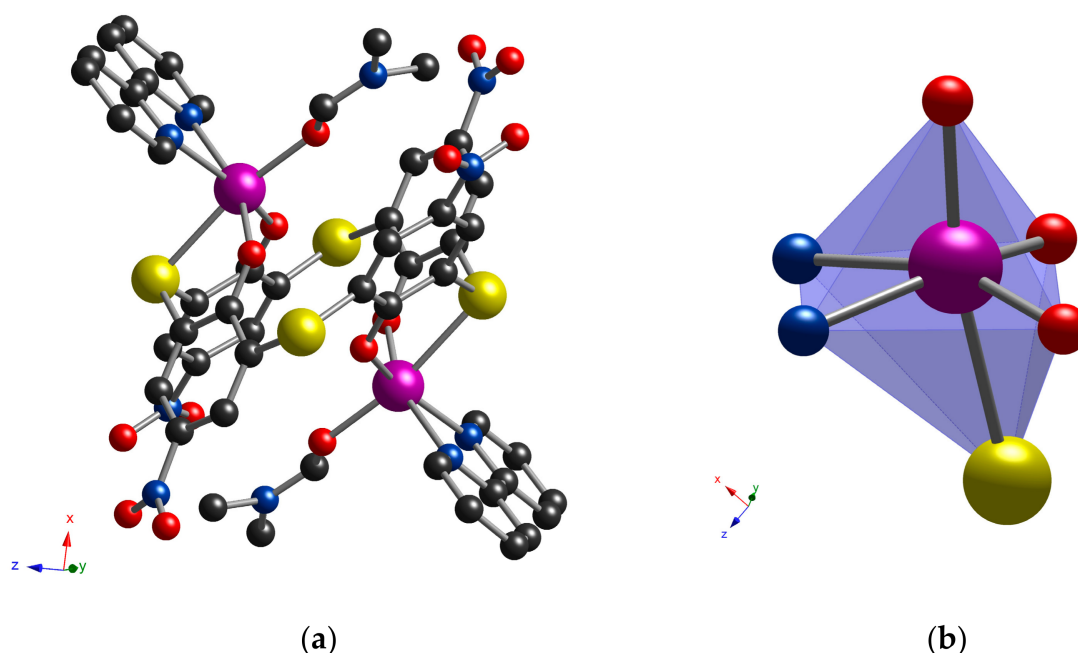


Figure 9. Crystal structure of **3** (a) and coordination environment of Mn(1) atom (b). The C-, N-, O-, Mn- and S-atoms are represented by black, blue, red, purple and yellow spheres, respectively. Hydrogen atoms are omitted for clarity.

The **bipy** ligand, providing both N-atoms for coordination with Mn(II) ions, acts as a bidentate chelate ligand. Two Mn(1)-N coordination bonds are found to be practically equivalent (see Table S1). The pyridyl moieties of **bipy** are lying in the same plane, which is identified by the corresponding dihedral angle equal to 1.77°.

The coordination of Mn(1) ions with one DMF molecule completes their octahedral coordination sphere. The 3D crystal packing of **3** is stabilized by a number of relatively cohesive intermolecular n/π-, CH/π-, and CH/O interactions, involving an O-atom of the nitro groups and aromatic systems of **bipy** pyridyl moieties and nitroaryl groups of the macrocycle backbone ($d_{O(42) \dots C_{6\text{centroid}}} = 3.066 \text{ \AA}$, $d_{O(61) \dots C(23)} = 3.083 \text{ \AA}$, $d_{C(19) \dots C_{6\text{centroid}}} = 3.628 \text{ \AA}$, $d_{O(62) \dots C(10)} = 3.639 \text{ \AA}$, respectively, see Figures 10 and S7).

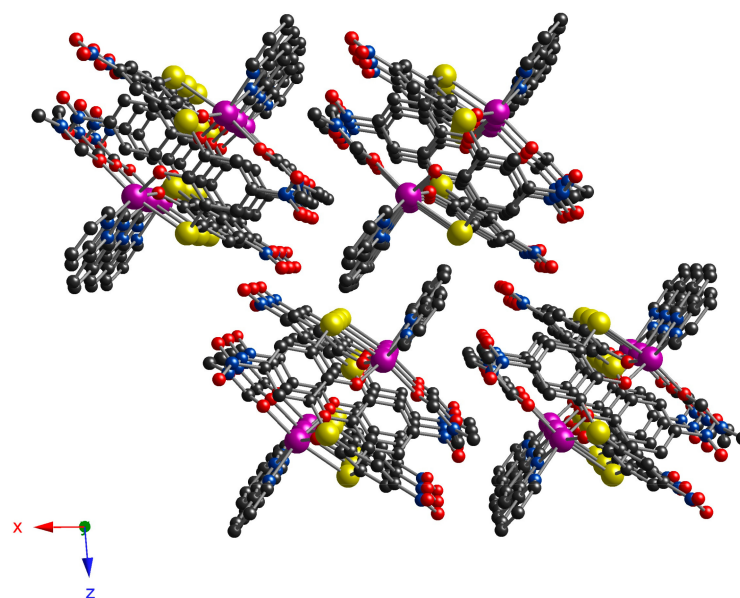


Figure 10. A portion of crystal packing of **3** (view along $0y$ axis).

4. Discussion

The use of the upper rim of di- and tetranitro derivatives of thiacalix[4]arene (**di-NO₂-TCA** and **tetra-NO₂-TCA**) as ligands in coordination with Mn(II) cations under self-assembly conditions produced the formation of three tetranuclear complexes (**1**, **2a** and **2b**) with a metal/ligand ratio equal to 2/1. For complexes **1** and **2a**, the macrocyclic ligands, adopting cone conformation, displayed a similar coordination mode, leading to the formation of a tetranuclear “sandwich”-like cluster where the cluster core was held by two macrocyclic ligands. For both **1** and **2a**, thiacalix[4]arene ligands displayed a similar coordination mode, offering four OSO-tridentate cavities for binding with four Mn(II) cations.

For **1** and **2a**, it was found that the appearance of the nitro groups at the upper rim of the thiacalix[4]arene ligands significantly changes depending on the structure of the tetranuclear cluster core, displaying the rhombic geometry and, consequently, presenting two types of non-equivalent manganese(II) atoms with O₄S₂ and O₆S₂ coordination environments, whereas for the earlier reported analogues, obtained using the thiacalix[4]arene ligands, the bearing electron donor groups such as *-t*-Bu and *-Ph*, and all four Mn(II) atoms forming the tetranuclear square cluster core were found to be equivalent [19,64]. Moreover, the involvement of **tetra-NO₂-TCA**, instead of **di-NO₂-TCA**, in the coordination of Mn(II) ions resulted in an increase of rhombic cluster core distortion, consisting in its compression along the axis connecting two Mn(1) atoms, which was caused by the weakening (elongation) of the coordination bonding between the O-atoms of the phenolate moieties. As a result, it induced the enhancement of the interaction between Mn(II) atoms with coordinated DMF molecules, leading to their partial intrusion into the complex. The emerged repulsion of coordinated solvent molecules and macrocyclic ligand in the coordination sphere of Mn(2) atoms resulted in the elongation of Mn-S coordination bonds (see Table S1).

There are only a few examples of octacoordinated Mn(II) cations in the metal–organic complexes displaying a N₈-, N₇O-, or O₈-coordination environment when the polydentate N- or O-donor ligands were used for the encapsulation of the single metal ion [65–70]. Thus, **1** and **2a** are the first examples of polynuclear complexes where the O-/S-donor ligands based on the thiacalix[4]arene macrocyclic platform are used for the stabilization of eight coordinate Mn(II) cations.

In contrast to **1** and **2a**, the macrocyclic ligand in **2b** is found to be adopted in a paco conformation, providing two kinds of coordination modes. The first one leads to the formation of a dinuclear cluster core, connecting two adjacent macrocyclic ligands, offering two OSO-tridentate cavities for coordination with two Mn(II) atoms. In addition, due to the

coordination of one inverted O-phenolate moiety, each molecule of the macrocyclic ligand binds with a single Mn(II) atom, which is located on one of the side positions of the complex. The formation of **2b** evidences the enhanced conformational flexibility of the macrocyclic platform of used **tetra-NO₂-TCA**, compared to **TCA**, which coordination chemistry has thoroughly explored. Moreover, the changing of the coordination pattern for **2b** leads to an enhanced value of the distortion parameter (CShM) of the O₄S₂ trigonal prismatic coordination sphere for Mn(II) ions (see Table S2). It should be noted that the observation of pentacoordinated Mn(II) atoms, connected with only one anion (phenolate group), is documented for the first time. Interestingly, the arrangement of complex molecules in the crystalline phase, displaying the non-centrosymmetrical space group *Pca*2₁ for **2b**, can expand the chemistry of thiacalix[4]arene ligands, adopted in *paco* conformation.

Finally, the addition of auxiliary ligand 2,2'-bipyridine led to the formation of complex **3** with **tetra-NO₂-TCA**, demonstrating an easy conformational transformation by adopting the 1.2-alternate conformation. The obtained result indicates that the involvement of chelating NN-donor ligand, possessing a high affinity to bind with Mn(II) cations, as shown earlier in the example of a CA-based cluster [71], instead of DMF molecules, in coordination with metal ions results in the destruction of the tetranuclear cluster core observed for **1** and **2a**, assumedly because of the steric hindrances.

5. Conclusions

The coordination of upper-rim substituted di- and tetranitro derivatives of thiacalix[4]arene (**di-NO₂-TCA** and **tetra-NO₂-TCA**) with Mn(II) cations under mild self-assembly conditions afforded the formation of four new polynuclear complexes, whose crystal structure was established using X-ray diffraction. Two complexes, **1** and **2a**, containing similar tetranuclear metallic clusters, presented two type of non-equivalent Mn(II) atoms with O₄S₂ and O₆S₂ coordination spheres, for which distortion was adjusted by varying the number of the nitro substituents on the upper rim of the macrocycle backbone. It was revealed that, for **1** and **2a**, thiacalix[4]arene ligands adopted in a *cone* conformation, in the case of **2b**, a *paco* conformation was observed for the macrocyclic ligand, leading to a non-centrosymmetric space group of the unit cell and the presence of four non-equivalent Mn(II) atoms within the complex species displaying an O₄S₂ or O₅ coordination environment. For **3**, the combination of 2,2'-bipyridine, **tetra-NO₂-TCA**, and MnCl₂ afforded dinuclear complex formation, where the macrocyclic ligand, adopting a 1.2-alternate conformation, was bound with two metal ions, displaying the N₂O₃S-coordination sphere.

The presented results evidence that the control over the coordination environment and the distortion of coordination sphere of manganese(II) cations as well as the conformation behavior of the macrocycle ligand can be achieved via the use of thiacalix[4]arene ligands containing electron-withdrawing groups, such as nitro substituents, from one side, and the addition of auxiliary ligands from another side. The magnetic and luminescence properties of the obtained coordination compounds are currently under investigation.

Supplementary Materials: The following supporting information can be downloaded at <https://www.mdpi.com/article/10.3390/cryst13071017/s1>. Figure S1: The thermal ellipsoids representation with 50% probability of asymmetric unit for **1** (a), **2a** (b), **2b** (c) and **3** (d). H-atoms are omitted for clarity; Figure S2: The macrocycle platform deformation resulting in the screwing of the opposite aryl units when binding with Mn (II) ions in **1** (a) and **2a** (b); Figure S3: For **1** and **2a**, inclusion of solvate DMF (a) or diethyl ether molecules (b) into the hydrophobic cavity of thiacalix[4]arene based ligands supported by CH/ π -interactions presented by blue dotted lines; Figure S4: Perpendicular orientation of the cluster molecules within the 2D layer for **1**; Figure S5: External CH/ π bonding between the co-crystallized molecules of diethyl ether and aryl units of macrocycle platform upon the crystal packing; Figure S6: For **2b**, the intermolecular CH/O(nitro) (a) and CH/ π (b) interactions involved in stabilization of the crystal packing; Figure S7: The noncovalent intermolecular interactions acting in stabilization of the crystal packing of **3**; Table S1: The coordination bonds lengths and angles for **1**, **2a**, **2b** and **3**; Table S2: CShM deviation values calculated by SHAPE program [63] for hexacoordinated Mn (II) atoms in **1**, **2a**, **2b** and **3**; Table S3: CShM deviation values calculated by SHAPE program [63]

for octacoordinated Mn atoms in **1** and **2a**; Table S4: CShM deviation values calculated by SHAPE program [63] for pentacoordinated Mn atoms in **2b**.

Author Contributions: Conceptualization, A.S.O., S.E.S. and I.S.A.; methodology, A.S.O., D.R.I. and A.T.G.; formal analysis, D.R.I., A.T.G. and P.V.D.; investigation, I.V.S., I.D.S. and A.S.A.; data curation, I.V.S., I.D.S., D.R.I. and A.T.G.; writing—original draft preparation, A.S.O., I.V.S. and S.E.S.; supervision, A.S.O., S.E.S. and I.S.A.; project administration, A.S.O., S.E.S. and I.S.A. All authors have read and agreed to the published version of the manuscript.

Funding: This research was funded by Russian Science Foundation, grant number 19-73-20035.

Data Availability Statement: Not applicable.

Acknowledgments: The authors are grateful to the Kurchatov Complex for Synchrotron and Neutron Investigations for the performance of the X-ray diffraction study of low diffracting single crystals of the obtained complexes, and to the Spectral-Analytical Center of FRC Kazan Scientific Center of RAS for technical support. The authors thank Mariia V. Kniازهva for help in the synthesis of the used macrocyclic ligands.

Conflicts of Interest: The authors declare no conflict of interest.

References

1. Gutsche, C.D. *Calixarenes Revised: Monographs in Supramolecular Chemistry*; The Royal Society of Chemistry: Cambridge, UK, 1998; Volume 6.
2. Asfari, Z.; Böhmer, V.; Harrowfield, J.; Vicens, J. (Eds.) *Calixarenes 2001*; Kluwer Academic: Dordrecht, The Netherlands, 2001.
3. Hosseini, M.W. *Calixarenes for Separations*; Lumetta, G.J., Rogers, R.D., Gopalan, A.S., Eds.; ACS Symposium Series; American Chemical Society: Washington, DC, USA, 2000.
4. Kumagai, H.; Hasegawa, M.; Miyanari, S.; Sugawa, Y.; Sato, Y.; Hori, T.; Ueda, S.; Kamiyama, H.; Miyano, S. Facile synthesis of p-tert-butylthiacalix[4]arene by the reaction of p-tert-butylphenol with elemental sulfur in the presence of a base. *Tetrahedron Lett.* **1997**, *38*, 3971–3972. [[CrossRef](#)]
5. Iki, N.; Kumagai, H.; Morohashi, N.; Ejima, K.; Hasegawa, M.; Miyanari, S.; Miyano, S. Selective oxidation of thiacalix[4]arenes to the sulfinyl- and sulfonylcalix[4]arenes and their coordination ability to metal ions. *Tetrahedron Lett.* **1998**, *39*, 7559–7562. [[CrossRef](#)]
6. Asfari, Z.; Bilyk, A.; Bond, C.; Harrowfield, J.M.; Koutsantonis, G.A.; Lengkeek, N.; Mocerino, M.; Skelton, B.W.; Sobolev, A.N.; Strano, S.; et al. Factors influencing solvent adduct formation by calixarenes in the solid state. *Org. Biomol. Chem.* **2004**, *2*, 387–396. [[CrossRef](#)] [[PubMed](#)]
7. Akdas, H.; Bringel, L.; Graf, E.; Hosseini, M.W.; Mislin, G.; Pansanel, J.; De Cian, A.; Fischer, J. Thiacalixarenes: Synthesis and Structural Analysis of Thiacalix[4]arene and of p-tert-Butylthiacalix[4]arene. *Tetrahedron Lett.* **1998**, *39*, 2311–2314. [[CrossRef](#)]
8. Mislin, G.; Graf, E.; Hosseini, M.W.; De Cian, A. Sulfone-calixarenes: A new class of molecular building block. *J. Chem. Soc. Chem. Commun.* **1998**, 1345–1346. [[CrossRef](#)]
9. Kajiwara, T.; Iki, N.; Yamashita, M. Transition metal and lanthanide cluster complexes constructed with thiacalix[n]arene and its derivatives. *Coord. Chem. Rev.* **2007**, *251*, 1734–1746. [[CrossRef](#)]
10. Kajiwara, T.; Kobashi, T.; Shinagawa, R.; Ito, T.; Takaishi, S.; Yamashita, M.; Iki, N. Highly Symmetrical Tetranuclear Cluster Complexes Supported by p-tert-Butylsulfonylcalix[4]arene as a Cluster-Forming Ligand. *Eur. J. Inorg. Chem.* **2006**, 1765–1770. [[CrossRef](#)]
11. Taylor, S.M.; Karotsis, G.; McIntosh, R.D.; Kennedy, S.; Teat, S.J.; Beavers, C.M.; Wernsdorfer, W.; Piligkos, S.; Dalgarno, S.J.; Brechin, E.K. A Family of Calix[4]arene-Supported $[\text{Mn}^{\text{III}}_2\text{Mn}^{\text{II}}_2]$ Clusters. *Chem. Eur. J.* **2011**, *17*, 7521–7530. [[CrossRef](#)]
12. Fuller, R.O.; Koutsantonis, G.A.; Ogden, M.I. Magnetic properties of calixarene-supported metal coordination clusters. *Coord. Chem. Rev.* **2020**, *402*, 213066. [[CrossRef](#)]
13. Aldoshin, S.M.; Antipin, I.S.; Ovcharenko, V.I.; Solov'eva, S.E.; Bogomyakov, A.S.; Korchagin, D.V.; Shilov, G.V.; Yur'eva, E.A.; Mushenok, F.B.; Bozhenko, K.V.; et al. Synthesis, structure, and properties of a new representative of the family of calix[4]arene-containing $[\text{Mn}^{\text{II}}_2\text{Mn}^{\text{III}}_2]$ -clusters. *Russ. Chem. Bull.* **2013**, *62*, 536–542. [[CrossRef](#)]
14. Karotsis, G.; Evangelisti, M.; Dalgarno, S.; Brechin, E. A Calix[4]arene 3d/4f Magnetic Cooler. *Angew. Chem. Int. Ed.* **2009**, *48*, 9928–9931. [[CrossRef](#)]
15. Kongzhao, S.; Jiang, F.; Qian, J.; Zhou, K.; Pang, J.; Basahel, S.; Mokhtar, M.; AL-Thabaiti, S.A.; Hong, M. Calix[4]arene-Based Clusters with μ_9 -Carbonato-Bridged Co^{II}_9 Cores. *Inorg. Lett.* **2014**, *1*, 1–8. Available online: <http://www.pubs.iscience.in/journal/index.php/il/article/view/116/64> (accessed on 14 January 2014).
16. Karotsis, G.; Kennedy, S.; Dalgarno, S.J.; Brechin, E.K. Calixarene supported enneanuclear Cu(II) clusters. *Chem. Commun.* **2010**, 46, 3884–3886. [[CrossRef](#)]
17. Sanz, S.; McIntosh, R.D.; Beavers, C.M.; Teat, S.J.; Evangelisti, M.; Brechin, E.K.; Dalgarno, S.J. Calix[4]arene-supported rare earth octahedra. *Chem. Commun.* **2012**, *48*, 1449–1451. [[CrossRef](#)]

18. Xing, T.; Frese, J.W.A.; Derbyshire, M.; Glenister, M.A.; Elsegood, M.R.J.; Redshaw, C. Trinuclear zinc calix[4]arenes: Synthesis, structure, and ring opening polymerization studies. *Dalton Trans.* **2022**, *51*, 11776–11786. [[CrossRef](#)]
19. Desroches, C.; Pilet, G.; Borshch, S.A.; Parola, S.; Luneau, D. Tetranuclear Manganese(II) Complexes of Thiocalixarene Macrocycles with Trigonal Prismatic Six-Coordinate Geometries: Synthesis, Structure, and Magnetic Properties. *Inorg. Chem.* **2005**, *44*, 9112–9120. [[CrossRef](#)]
20. Xiong, K.-C.; Jiang, F.-L.; Gai, Y.-L.; Yuan, D.-Q.; Han, D.; Ma, J.; Zhang, S.-Q.; Hong, M.-C. Chlorine-Induced Assembly of a Cationic Coordination Cage with a μ_5 -Carbonato-Bridged Mn^{II}_{24} Core. *Chem. Eur. J.* **2012**, *18*, 5536–5540. [[CrossRef](#)]
21. Guan, Z.-J.; Zeng, J.-L.; Nan, Z.-A.; Wan, X.-K.; Lin, Y.-M.; Wang, Q.-M. Thiocalix[4]arene: New protection for metal nanoclusters. *Sci. Adv.* **2016**, *2*, e160032. [[CrossRef](#)]
22. Wang, Z.; Su, H.F.; Gong, Y.W.; Qu, Q.P.; Bi, Y.F.; Tung, C.H.; Sun, D.; Zheng, L.S. A hierarchically assembled 88-nuclei silver-thiocalix[4]arene nanocluster. *Nat. Commun.* **2020**, *11*, 308. [[CrossRef](#)]
23. Aldoshin, S.M.; Antipin, I.S.; Kniazeva, M.V.; Korchagin, D.V.; Morgunov, R.B.; Ovsyannikov, A.S.; Pali, A.V.; Sanina, N.A.; Shilov, G.V.; Solovieva, S.E. Synthesis, Structure and Magnetic Properties of Mn_2Tb_2 Tetranuclear Complex with p-tert-Butylthiocalix[4]arene. *Isr. J. Chem.* **2020**, *60*, 600–606. [[CrossRef](#)]
24. Liu, J.-Y.; Sheng, T.-P.; Li, C.; Wang, Z.; Dai, F.-R.; Chen, Z.-N. Iodine Adsorption via Porous Molecular Solids Based on Coordination Containers Derived from Naphthalene-1,8-dicarboxylate. *Cryst. Growth Des.* **2022**, *22*, 3182–3189. [[CrossRef](#)]
25. Bi, Y.; Wang, X.-T.; Liao, W.; Wang, X.; Deng, R.; Zhang, H.; Gao, S. Thiocalix[4]arene-Supported Planar Ln_4 ($Ln = Tb^{III}, Dy^{III}$) Clusters: Toward Luminescent and Magnetic Bifunctional Materials. *Inorg. Chem.* **2009**, *48*, 11743–11747. [[CrossRef](#)] [[PubMed](#)]
26. Liu, C.-M.; Zhang, D.-Q.; Hao, X.; Zhu, D.-B. Syntheses, Crystal Structures, and Magnetic Properties of Two p-tert-Butylsulfonycalix[4]arene Supported Cluster Complexes with a Totally Disordered $Ln_4(OH)_4$ Cubane Core. *Cryst. Growth Des.* **2012**, *12*, 2948–2954. [[CrossRef](#)]
27. Kajiwar, T.; Yokozawa, S.; Ito, T.; Iki, N.; Morohashi, N.; Miyano, S. Sulfonycalix[4]arene as a Bis-Tridentate Facial Ligand: Syntheses and Structures of Dinuclear Complexes, $[M_2(L)(H_2O)_2(dmf)_4]$ ($M = Co(II), Ni(II)$; $H_4L = p$ -tert-Butylsulfonycalix[4]arene). *Chem. Lett.* **2001**, *30*, 6–7. [[CrossRef](#)]
28. Lamouchi, M.; Jeanneau, E.; Novitchi, G.; Luneau, G.; Brioude, A.; Desroches, C. Polynuclear Complex Family of Cobalt(II)/Sulfonycalixarene: One- Pot Synthesis of Cluster Salt $[Co_{14}^{II}]^+ [Co_4^{II}]^-$ and Field-Induced Slow Magnetic Relaxation in a Six-Coordinate Dinuclear Cobalt(II)/Sulfonycalixarene Complex. *Inorg. Chem.* **2014**, *53*, 63–72. [[CrossRef](#)]
29. Ovsyannikov, A.; Solovieva, S.; Antipin, I.; Ferlay, S. Coordination Polymers based on calixarene derivatives: Structures and properties. *Coord. Chem. Rev.* **2017**, *352*, 151–186. [[CrossRef](#)]
30. Ovsyannikov, A.S.; Khariushin, I.V.; Solovieva, S.E.; Antipin, I.S.; Komiya, H.; Marets, N.; Tanaka, H.; Ohmagari, H.; Hasegawa, M.; Zakrzewski, J.J.; et al. Mixed Tb/Dy coordination ladders based on tetra(carboxymethyl)thiocalix[4]arene: A new avenue towards luminescent molecular nanomagnets. *RSC Adv.* **2020**, *10*, 11755–11765. [[CrossRef](#)]
31. Ovsyannikov, A.S.; Ferlay, S.; Solovieva, S.E.; Antipin, I.S.; Konovalov, A.I.; Kyritsakas, N.; Hosseini, M.W. Molecular tectonics: High dimensional coordination networks based on methylenecarboxylate-appended tetramercaptothiocalix[4]arene in the 1,3-alternate conformation. *CrystEngComm* **2018**, *20*, 1130–1140. [[CrossRef](#)]
32. Suffren, Y.; O’Toole, N.; Hauser, A.; Jeanneau, E.; Brioude, A.; Desroches, C. Discrete Polynuclear Manganese(II) Complexes with Thiocalixarene Ligands: Synthesis, Structures and Photophysical Properties. *Dalton Trans.* **2015**, *44*, 7991–8000. [[CrossRef](#)]
33. O’Toole, N.; Lecourt, C.; Suffren, Y.; Hauser, A.; Khrouz, L.; Jeanneau, E.; Brioude, A.; Luneau, D.; Desroches, C. Photogeneration of Manganese(III) from Luminescent Manganese(II) Complexes with Thiocalixarene Ligands: Synthesis, Structures and Photophysical Properties. *Eur. J. Inorg. Chem.* **2019**, 73–78. [[CrossRef](#)]
34. Lecourt, C.; Suffren, Y.; Jeanneau, E.; Luneau, D.; Desroches, C. Mono-, Di-, and Tetranuclear Manganese(II) Complexes with p-Phenylsulfonycalix[4]arene Macrocycles as Ligand Antennas: Synthesis, Structures, and Emission Properties. *Cryst. Growth Des.* **2022**, *22*, 2279–2288. [[CrossRef](#)]
35. Lamouchi, M.; Jeanneau, E.; Pillonnet, A.; Brioude, A.; Martini, M.; Stéphan, O.; Meganem, F.; Novitchi, G.; Luneau, D.; Desroches, C. Tetranuclear Manganese(II) Complexes of Sulfonycalix[4]Arene Macrocycles: Synthesis, Structure, Spectroscopic and Magnetic Properties. *Dalton Trans.* **2012**, *41*, 2707–2713. [[CrossRef](#)]
36. Hang, X.; Bi, Y. Thiocalix[4]arene-supported molecular clusters for catalytic applications. *Dalton Trans.* **2021**, *50*, 3749–3758. [[CrossRef](#)]
37. Bi, Y.; Du, S.; Liao, W. Thiocalixarene-based nanoscale polyhedral coordination cages. *Coord. Chem. Rev.* **2014**, *276*, 61–72. [[CrossRef](#)]
38. Geng, D.; Han, X.; Bi, Y.; Qin, Y.; Li, Q.; Huang, L.; Zhou, K.; Song, L.; Zheng, Z. Merohedral icosahedral M_{48} ($M = \frac{1}{4} Co^{II}, Ni^{II}$) cage clusters supported by thiocalix[4]arene. *Chem. Sci.* **2018**, *9*, 8535–8541. [[CrossRef](#)]
39. Liang, Y.; Li, E.; Wang, K.; Guan, Z.-J.; He, H.-H.; Zhang, L.; Zhou, H.-C.; Huang, F.; Fang, Y. Organo-macrocyclic-containing hierarchical metal-organic frameworks and cages: Design, structures, and applications. *Chem. Soc. Rev.* **2022**, *51*, 8378–8405. [[CrossRef](#)]
40. Khariushin, I.V.; Ovsyannikov, A.S.; Baudron, S.A.; Ward, J.S.; Kiesilä, A.; Rissanen, K.; Kalenius, E.; Kovalenko, K.A.; Fedin, V.P.; Solovieva, S.E.; et al. Selective gas adsorption by calixarene-based porous octahedral M_{32} coordination cages. *Chem. Commun.* **2022**, *58*, 13628–13631. [[CrossRef](#)]

41. Kniazeva, M.V.; Ovsyannikov, A.S.; Nowicka, B.; Kyritsakas, N.; Samigullina, A.I.; Gubaidullin, A.T.; Islamov, D.R.; Dorovatovskii, P.V.; Popova, E.V.; Kleshnina, S.R.; et al. Porous nickel and cobalt hexanuclear ring-like clusters built from two different kind of calixarene ligands—New molecular traps for small volatile molecules. *CrystEngComm* **2022**, *24*, 330–340. [[CrossRef](#)]
42. Kniazeva, M.V.; Ovsyannikov, A.S.; Samigullina, A.I.; Islamov, D.R.; Gubaidullin, A.T.; Dorovatovskii, P.V.; Lazarenko, V.A.; Solovieva, S.E.; Antipin, I.S.; Ferlay, S. Impact of flexible succinate connectors on the formation of tetrasulfonylcalix[4]arene based nano-sized polynuclear cages: Structural diversity and induced chirality study. *CrystEngComm* **2022**, *24*, 628–638. [[CrossRef](#)]
43. Pullen, S.; Tessarolo, J.; Clever, G.H. Increasing structural and functional complexity in self-assembled coordination cages. *Chem. Sci.* **2021**, *12*, 7269–7293. [[CrossRef](#)] [[PubMed](#)]
44. Shi, C.; Chen, M.; Han, X.; Bi, Y.; Huang, L.; Zhou, K.; Zheng, Z. Thiacalix[4]arene-supported tetradecanuclear cobalt nanocage cluster as precursor to synthesize CoO/Co₉S₈@CN composite for supercapacitor Application. *Inorg. Chem. Front.* **2018**, *5*, 1329–1335. [[CrossRef](#)]
45. Liu, M.; Liao, W. Bridging calixarene-based {Co₄} units into a square or belt with aromatic dicarboxylic acids. *CrystEngComm* **2012**, *14*, 5727–5729. [[CrossRef](#)]
46. Kniazeva, M.V.; Ovsyannikov, A.S.; Islamov, D.R.; Samigullina, A.I.; Gubaidullin, A.T.; Dorovatovskii, P.V.; Solovieva, S.E.; Antipin, I.S.; Ferlay, S. Crystalline Assembly and Solvent-induced Solid-state Transformation of 1D Zigzag Chains Based on Sulfonylcalix[4]arene Trinuclear Co(II) and Zn(II) Clusters. *Eur. J. Inorg. Chem.* **2022**, *32*, e202200464. [[CrossRef](#)]
47. Su, K.; Jiang, F.; Qian, J.; Pang, J.; Hu, F.; Bawaked, S.M.; Mokhtar, M.; Al-Thabaitic, S.A. Bridging different Co₄-calix[4]arene building blocks into grids, cages and 2D polymers with chiral camphoric acid. *CrystEngComm* **2015**, *17*, 1750–1753. [[CrossRef](#)]
48. Huang, C.; Liao, W. A porous 2D cobalt-sulfonylcalix[4]arene coordination polymer for gas adsorption. *J. Mol. Struct.* **2021**, *1237*, 130392. [[CrossRef](#)]
49. Hu, X.; Shi, H.; Shi, X.; Zhu, Z.; Sun, Q.; Li, Y.; Yang, H. Selective nitration of thiacalix[4]arene and an investigation of its acid–base properties with a chemometric method. *Bull. Chem. Soc. J.* **2005**, *78*, 138–141. [[CrossRef](#)]
50. Hu, X.; Zhu, Z.; Shen, T.; Shi, X.; Ren, J.; Sun, Q. Synthesis of the tetranitro derivative of thiacalix[4]arene and its acid-base properties. *Can. J. Chem.* **2004**, *82*, 1266–1270. [[CrossRef](#)]
51. Lazarenko, V.A.; Dorovatovskii, P.V.; Zubavichus, Y.V.; Burlov, A.S.; Koshchienko, Y.V.; Vlasenko, V.G.; Khrustalev, V.N. High-throughput small-molecule crystallography at the ‘Belok’ beamline of the Kurchatov synchrotron radiation source: Transition metal complexes with azomethine ligands as a case study. *Crystals* **2017**, *7*, 325. [[CrossRef](#)]
52. Svetogorov, R.D.; Dorovatovskii, P.V.; Lazarenko, V.A. Belok/XSA diffraction beamline for studying crystalline samples at Kurchatov Synchrotron Radiation Source. *Cryst. Res. Technol.* **2020**, *55*, 1900184. [[CrossRef](#)]
53. Kabsch, W. XDS. *Acta Crystallogr.* **2010**, *D66*, 125–132. [[CrossRef](#)]
54. Sheldrick, G.M. SHELXT: Integrating space group determination and structure solution. *Acta Crystallogr.* **2015**, *A71*, 3–8. [[CrossRef](#)]
55. Dolomanov, O.V.; Bourhis, L.J.; Gildea, R.J.; Howard, J.A.K.; Puschmann, H.J. OLEX2: A Complete Structure Solution, Refinement and Analysis Program. *Appl. Cryst.* **2009**, *42*, 339–341. [[CrossRef](#)]
56. Spek, A.L. *PLATON, a Multipurpose Crystallographic Tool*; Utrecht University: Utrecht, The Netherlands, 2001.
57. Sheldrick, G.M. A Short History of SHELX. *Acta Crystallogr.* **2007**, *A64*, 112–122. [[CrossRef](#)]
58. Sheldrick, G. *SADABS, Program for Empirical X-ray Absorption Correction*; Bruker-Nonius: Madison, WI, USA, 2004.
59. Sheldrick, G. *SHELXTL V.6.12, Structure Determination Software Suite*; Bruker AXS: Madison, WI, USA, 2000.
60. *APEX3 Program, Version 2018.7-2*; Bruker AXS Inc.: Madison, WI, USA, 2016.
61. Farrugia, L.J. WinGX suite for small-molecule single-crystal crystallography. *J. Appl. Crystallogr.* **1999**, *32*, 837–838. [[CrossRef](#)]
62. Macrae, C.F.; Edgington, P.R.; McCabe, P.; Pidcock, E.; Shields, G.P.; Taylor, R.; Towler, M.; Van De Streek, J. Mercury: Visualization and analysis of crystal structures. *J. Appl. Crystallogr.* **2006**, *39*, 453–457. [[CrossRef](#)]
63. Llunell, M.; Casanova, D.; Cirera, J.; Bofill, J.M.; Alemany, P.; Alvarez, S.; Pinsky, M.; Avnir, D. *SHAPE*; Version 2.3; University of Barcelona: Barcelona, Spain; Hebrew University of Jerusalem: Jerusalem, Israel, 2013.
64. Bi, Y.; Liao, W.; Wang, X.; Wang, X.; Zhang, H. Mn₄-hinged bithiacalix[4]arenes accommodating fullerenes. *Dalton Trans.* **2011**, *40*, 1849–1851. [[CrossRef](#)]
65. Neupert-Laves, K.; Dobler, M. Crystal Structure of Metal-Ion Complexes with neutral noncyclic Ionophores. *Helv. Chim. Acta* **1977**, *60*, 1861–1871. [[CrossRef](#)]
66. Reid, H.O.; Kahwa, I.A.; White, A.J.; Williams, D.J. Intense Photosensitized Emission from Stoichiometric Compounds Featuring Mn²⁺ in Seven- and Eightfold Coordination Environments. *Inorg. Chem.* **1998**, *37*, 3868–3873. [[CrossRef](#)]
67. Dang, D.B.; Bai, Y.; Duan, C. Crystal Structure and Magnetic Properties of a Novel Octa-coordinated Manganese(II) Complex. *J. Chem. Crystallogr.* **2008**, *38*, 557–560. [[CrossRef](#)]
68. Wang, S.; Westmoreland, T.D. Correlation of Relaxivity with Coordination Number in Six-, Seven-, and Eight-Coordinate Mn(II) Complexes of Pendant-Arm Cyclen Derivatives. *Inorg. Chem.* **2009**, *48*, 719–727. [[CrossRef](#)]
69. Dube, K.S.; Harrop, T.C. Structure and properties of an eight-coordinate Mn(ii) complex that demonstrates a high water relaxivity. *Dalton Trans.* **2011**, *40*, 7496–7498. [[CrossRef](#)] [[PubMed](#)]

70. Cieslik, P.; Comba, P.; Dittmar, B.; Ndiaye, D.; Tóth, É.; Velmurugan, G.; Wadepohl, H. Exceptional Manganese(II) Stability and Manganese(II)/Zinc(II) Selectivity with Rigid Polydentate Ligands. *Angew. Chem. Int. Ed.* **2022**, *61*, e202115580. [[CrossRef](#)] [[PubMed](#)]
71. Aldoshin, S.M.; Antipin, I.S.; Solovieva, S.E.; Sanina, N.A.; Korchagin, D.V.; Shilov, G.V.; Mushenok, F.B.; Utenyshev, A.N.; Bozhenko, K.V. Experimental and theoretical study of the influence of peripheral environment on magnetic properties of tetranuclear manganese skeleton in new representatives of calix[4]arene-containing $[\text{Mn}^{\text{II}}_2\text{Mn}^{\text{III}}_2]$ clusters. *J. Mol. Struct.* **2015**, *1081*, 217–223. [[CrossRef](#)]

Disclaimer/Publisher's Note: The statements, opinions and data contained in all publications are solely those of the individual author(s) and contributor(s) and not of MDPI and/or the editor(s). MDPI and/or the editor(s) disclaim responsibility for any injury to people or property resulting from any ideas, methods, instructions or products referred to in the content.